



Article

Evaluating the Removal of the Antibiotic Cephalexin from Aqueous Solutions Using an Adsorbent Obtained from Palm Oil Fiber

Nancy Acelas ^{1,*} , Sandra M. Lopera ², Jazmín Porras ³ and Ricardo A. Torres-Palma ² 

¹ Grupo de Materiales con Impacto, MAT&MPAC, Facultad de Ciencias Básicas, Universidad de Medellín, Medellín 050010, Colombia

² Grupo de Investigación en Remediación Ambiental y Biocatálisis (GIRAB), Instituto de Química, Facultad de Ciencias Exactas y Naturales, Universidad de Antioquia UdeA, Calle 70 No. 52-21, Medellín 050010, Colombia; samy2810@gmail.com (S.M.L.); ricardo.torres@udea.edu.co (R.A.T.-P.)

³ Grupo de Investigaciones Biomédicas Uniremington, Facultad de Ciencias de la Salud, Corporación Universitaria Remington (Uniremington), Calle 51 No. 51-27, Medellín 050010, Colombia; jazmin.porras@uniremington.edu.co

* Correspondence: nyacelas@udem.edu.co; Tel.: +57-(4)-340-52-78

Abstract: This study aimed to understand the adsorption process of cephalexin (CPX) from aqueous solution by a biochar produced from the fiber residue of palm oil. Scanning electron microscopy, Fourier transform infrared spectroscopy, Boehm titration, and the point of zero charge were used to characterize the morphology and surface functional groups of the adsorbent. Batch tests were carried out to evaluate the effects of the solution pH, temperature, and antibiotic structure. The adsorption behavior followed the Langmuir model and pseudo-second-order model with a maximum CPX adsorption capacity of 57.47 mg g⁻¹. Tests on the thermodynamic behavior suggested that chemisorption occurs with an activation energy of 91.6 kJ mol⁻¹ through a spontaneous endothermic process. Electrostatic interactions and hydrogen bonding represent the most likely adsorption mechanisms, although π - π interactions also appear to contribute. Finally, the CPX removal efficiency of the adsorbent was evaluated for synthetic matrices of municipal wastewater and urine. Promising results were obtained, indicating that this adsorbent can potentially be applied to purifying wastewater that contains trace antibiotics.

Keywords: adsorption; cephalexin; wastewater; biochar; isotherm; kinetics



Citation: Acelas, N.; Lopera, S.M.; Porras, J.; Torres-Palma, R.A. Evaluating the Removal of the Antibiotic Cephalexin from Aqueous Solutions Using an Adsorbent Obtained from Palm Oil Fiber. *Molecules* **2021**, *26*, 3340. <https://doi.org/10.3390/molecules26113340>

Academic Editor: João Valente Nabais

Received: 26 March 2021

Accepted: 1 May 2021

Published: 2 June 2021

Publisher's Note: MDPI stays neutral with regard to jurisdictional claims in published maps and institutional affiliations.



Copyright: © 2021 by the authors. Licensee MDPI, Basel, Switzerland. This article is an open access article distributed under the terms and conditions of the Creative Commons Attribution (CC BY) license (<https://creativecommons.org/licenses/by/4.0/>).

1. Introduction

Antibiotics are indispensable products for human life, and their consumption has increased to combat the spread of infectious diseases in humans and animals [1]. However, 30–90% of consumed antibiotics are not metabolized in the body and are discharged into aquatic systems as active compounds [2]. Cephalexin (CPX) is an antibiotic of the cephalosporin family, which is the second-most consumed group of antibiotics worldwide [3], and is normally used to treat respiratory and urinary infections [4]. The discharge of contaminated water from pharmaceutical facilities, hospitals, homes, and agro-industrial facilities containing pharmaceuticals such as CPX into the environment can have adverse impacts on human health, increase antibiotic resistance, and inhibit the growth of algae and beneficial microorganisms in the environment [5]. Therefore, it is important to explore efficient and cost-effective technologies to remove antibiotics from polluted water.

Adsorption is a promising and available technique for removing many contaminants in water. For example, biochar is a carbon-rich material produced from biomass that is excellent at removing organic contaminants [2,6–11]. Biochar has a porous structure, high aromaticity, and various functionalities that confer the capability for different interactions and coupling with antibiotic molecules [5]. Several oxygenated functional groups on

its surface, including alcohols, carboxylic acids, phenols, and ethers, allow interactions such as π - π electron donor-acceptor interactions, electrostatic interactions, and hydrogen bonding that have been established as major adsorption mechanisms between antibiotics and biochar [6].

One of the most popular methods for producing low-cost biochar adsorbents is through pyrolysis and subsequent chemical activation of the biomass waste. This method also helps mitigate issues with biomass waste disposal. Therefore, several agro-industrial residues (e.g., alligator weed [2], walnut shells [7], bamboo waste [1], tea industry wastes [8], *Albizia lebbbeck* seed pods [9], pistachio shells [10], alfalfa hay [11], and rice husks [5,12,13]) have been studied for their ability to remove antibiotics and other pharmaceuticals from water. Most of these studies have focused on determining the maximum adsorption capacities of these residues. A wide range of adsorption capacities has been reported that depends on both the type of agro-industrial residue and the preparation procedure [5,12,13]. The use of palm oil residues as adsorbents is of special interest as the palm oil agro-industry generates a significant amount of residual biomass (~87 million t/y) [14]. Several studies have demonstrated that biochar produced from palm oil and other agro-industrial residues is an effective adsorbent for removing heavy metals [15–17], dyes [18,19], pharmaceuticals [20–23], and other organic pollutants [24] from aqueous systems.

Thus, the objective of this study was to produce and apply biochar derived from fiber and shell residues of palm oil to remove CPX from water. Batch experiments were performed to investigate the CPX adsorption behavior of biochar. The effects of the solution pH, temperature, matrix, and antibiotic structure were evaluated. The adsorption kinetics, isotherm, and thermodynamics were evaluated to characterize the adsorption behavior in detail. Finally, structural properties of the adsorbent, including the pore size, volume, and surface functional groups, were analyzed to clarify the CPX adsorption process of biochar produced from palm oil residue.

2. Results and Discussion

2.1. CPX Removal Performance of Each Adsorbent

The differences in the adsorption properties of F and S were evaluated to determine the influences of the original material and activation process. Batch-type experiments were carried out where each adsorbent was placed in contact with a solution with 20 mg L⁻¹ of CPX. As shown in Figure 1, F_{Zn} has the highest CPX removal efficiency at 74.1%, while S_{Zn} and F_{HA} had similar removal efficiencies of 17.5% and 17.4%, respectively.

This behavior can be associated with the nature of the prepared adsorbent and is characterized by the pH at PZC (pH_{PZC}), which is a parameter for identifying the variation in the surface charge of the adsorbent with the pH. If pH_{PZC} is known, then the pH values at which the biochar would have a positive or negative charge can be determined. This is useful for determining the pH conditions and chemical structure of the pollutant that would favor the adsorption process. As presented in Table 1, F_{Zn}, S_{Zn}, and F_{HA} had pH_{PZC} values of 4.0, 2.3, and 4.8, respectively. At the pH of the experiment (pH = 6.5), all of these adsorbents would have a negative surface charge to interact with the positive charge of CPX, which would be in zwitterionic form (pK_{a1} 2.56 and pK_{a1} 6.88). Thus, all adsorbents had the potential for electrostatic interaction. This indicates that pH_{PZC} by itself does not explain the behavior of adsorbents during the CPX adsorption process. Therefore, the morphology and surface area also needed to be considered.

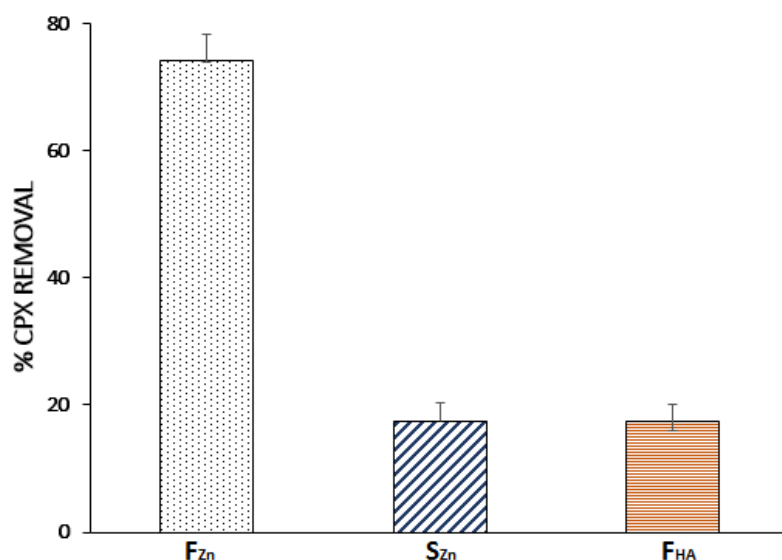


Figure 1. Performance of each adsorbent material for cephalixin (CPX) removal (adsorption conditions: (CPX): 20 mg L⁻¹, adsorbent doses: 1.6 g L⁻¹; time: 60 min, pH: 6.5).

Table 1. Physical and chemical surface properties. PZC, point of zero charge.

Adsorbent Material	Surface Area (m ² /g)	pH _{PZC}		
F _{Zn}	835.3	4.0		
S _{Zn}	575.1	2.3		
F _{HA}	14.8	4.8		
Acid groups F _{Zn}	Carboxylic	Phenolic	Lactones	
Value (mmol g ⁻¹)	1.65	0.20	0.15	

The results with the BET method showed that the specific surface areas of F_{Zn}, S_{Zn}, and F_{HA} were 835.3, 575.1, and 14.8 m² g⁻¹, respectively (see Table 1).

These results indicate that the activating agent is a fundamental key for the modification of biomass to produce an activated carbon. As shown in Figure 2, adsorbents produced with ZnCl₂ as the activating agent had a more porous structure than the adsorbent produced with H₃PO₄. These pores can be partially attributed to the effect of ZnCl₂, which is a dehydrating reagent that promotes the decomposition of carbonaceous materials, restricts the formation of tars, and induces carbon aromatization [15]. These observations are in agreement with the surface areas from the BET analysis, where F_{Zn} had the largest surface area. This may be directly correlated with a higher CPX removal efficiency.

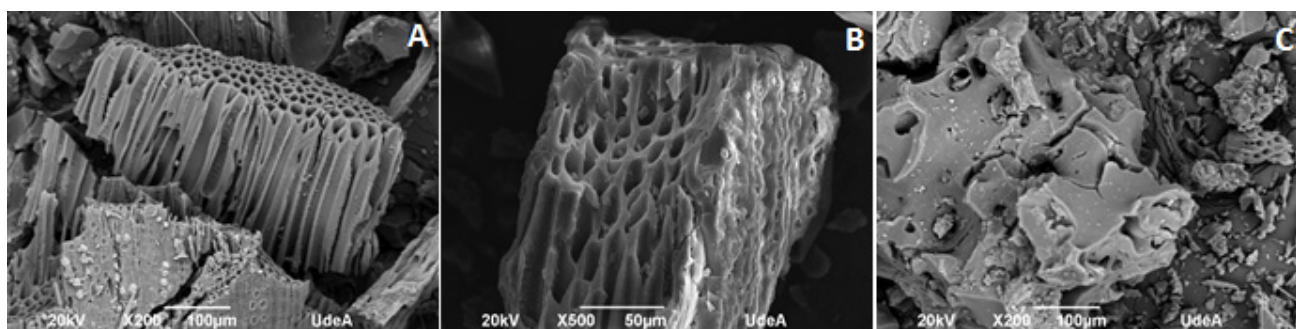


Figure 2. Scanning electron microscopy (SEM) micrographs of the adsorbent materials: (A) F_{Zn} (fiber activated with ZnCl₂); (B) S_{Zn} (shell activated with ZnCl₂); and (C) F_{HA} (fiber activated with phosphoric acid).

However, the surface area is not the only determining factor for the CPX adsorption process, because S_{Zn} had a surface area 39 times greater than that of F_{HA} , but both adsorbents had similar CPX removal efficiencies (~20%). This indicates that the surface functional groups play an important role in the adsorption process.

Figure S1 (Supporting Information) shows the infrared (IR) spectra for the three adsorbents before and after the CPX adsorption process. Both F_{Zn} and F_{HA} had carboxylic acid and phenol functional groups, as evidenced by the amplitude of the signal at 3600 cm^{-1} , corresponding to the $-OH$ functional group. Here, S_{Zn} did not have a large amplitude. After adsorption, the signal at 3600 cm^{-1} became less intense for F_{Zn} , indicating that CPX may have interacted with these oxygenated functional groups. Boehm titration was carried out (Table 1) to verify and quantify the acid groups on F_{Zn} , which had the highest CPX removal efficiency. The carboxylic acid groups were more abundant than the phenols and lactones by 8.3 and 11 times, respectively.

The above results indicate that both the activating method and biomass type can considerably affect CPX adsorption because they can be varied to produce adsorbents with different physicochemical characteristics such as the morphology, functional groups, and surface area. These results suggest that effects other than the surface area influence the adsorption and that the surface functional groups may be the main factor for CPX removal.

The pH is known as a key factor in adsorption processes, and it influences the chemical nature of the functional groups and contaminant. Thus, the effects of the functional groups and pH on CPX adsorption were evaluated in further detail. F_{Zn} was selected for further analysis because it was the adsorbent with the highest CPX removal efficiency.

2.2. Effect of pH on CPX Adsorption

The solution pH influences the surface charge and surface functional groups of the adsorbent as well as the CPX structure (related to pKa). Thus, pH was varied to evaluate the effect on CPX removal, with the results shown in Figure 3. The CPX removal decreased as the pH was increased from 2 to 12. At pH values of 2–6, the CPX removal was around 90%; at pH values of >6.5, the CPX removal decreased to 20% at pH 9.2 and 6% at pH 11.5. In control experiments, hydrolysis of CPX at these pH values was discarded (data not shown).

This relationship between CPX removal and solution pH can be explained by the properties of the adsorbent, such as the surface charge ($pH_{pzc} \sim 4.0$) and surface functional groups, and CPX, such as its chemical structure and acid–base properties (pK_a values) (Figure 3) [13].

The similar levels of CPX removal from pH 2 to 6 may be related to the fact that the adsorbent had both positive and negative charges at these pH values. At pH 2, the adsorbent was slightly positive, and at pH 6, the adsorbent was slightly negative. Hence, within this pH range, CPX was in the zwitterionic form; it had both positive and negative charges, which favored adsorption by electrostatic interactions. These results indicate that this adsorbent favors the adsorption of charged pollutants. If the pollutant is positively charged, adsorption occurs over a wide pH range, favoring $pH < 8$. However, if the contaminant is negatively charged, the adsorption decreases when $pH > 8$. Similar reports [25] have shown that the CPX removal efficiency increases with decreasing pH, which agrees with the results of the present study. This indicates that, in addition to the electrostatic charge, the interaction between surface functional groups is also important for the CPX removal efficiency.

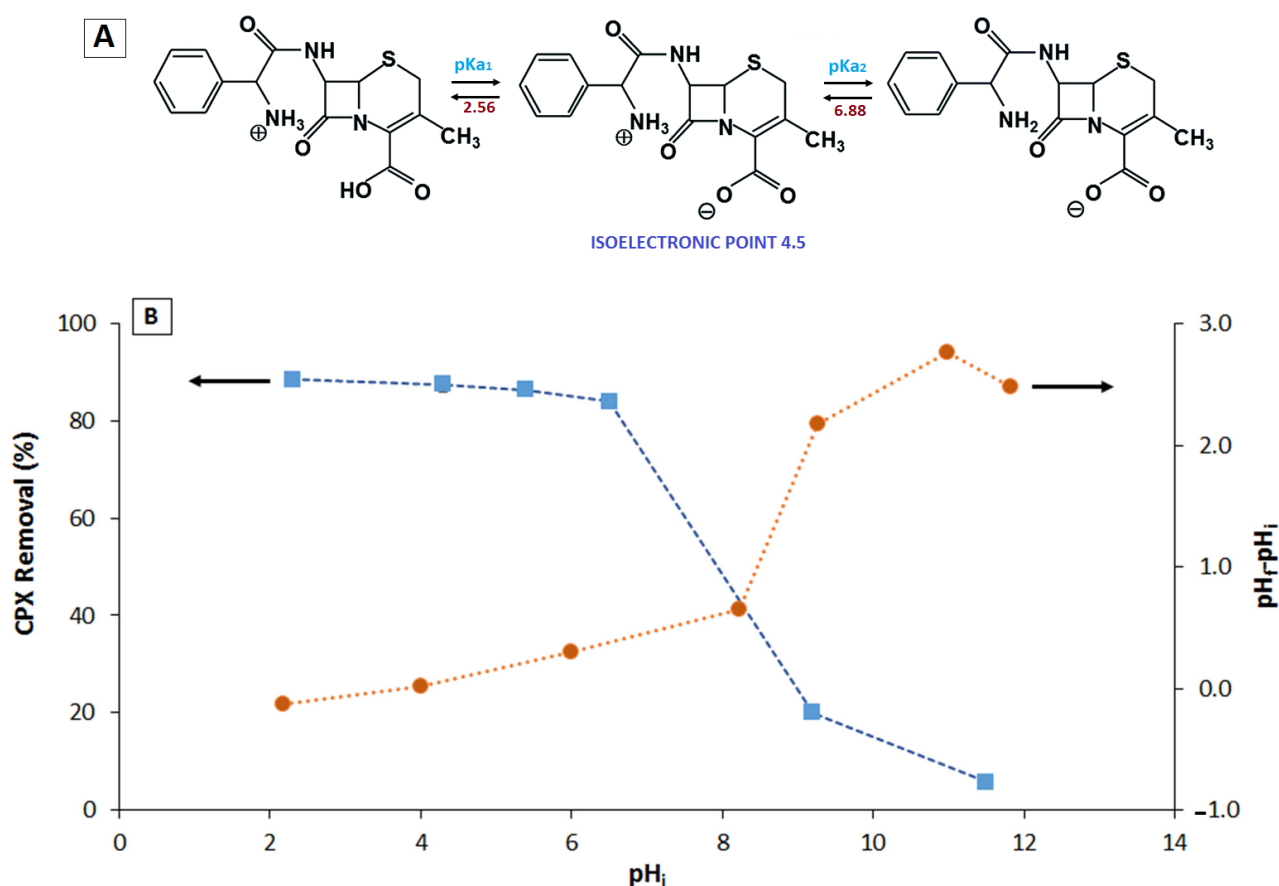


Figure 3. (A) Cephalexin ionization states and (B) (left) the effect of the solution pH on the CPX removal using F_{Zn} (adsorption conditions (CFX): 20 mg L⁻¹, adsorbent doses: 1.6 g L⁻¹, time: 60 min); (B) (right) point of zero charge (PZC) for the material.

2.3. Effect of Chemical Structure on CPX Adsorption

Changes to adsorption due to pH are affected by the structure of the antibiotic, which may improve or worsen the interaction between the adsorbate and adsorbent. The influence of the chemical structure of the pharmaceutical on the removal process was evaluated to clarify its interactions with the adsorbent. As shown in Figure 4, three pharmaceuticals with different chemical structures were tested for their removal by F_{Zn}, i.e., naproxen (NPX), acetaminophen (ACE), and cephalexin (CPX).

NPX and CPX followed similar trends with removal efficiencies of ~90% during the first 7 min of treatment, after which adsorption equilibrium was achieved. Meanwhile, ACE had a maximum removal efficiency of around 20%. To explain these results, the pH_{PZC} of F_{Zn} and pK_a of the pharmaceuticals were considered. Under natural pH conditions (4.0–5.0), the pK_a values indicate that the pharmaceuticals have the following chemical form: CPX is principally zwitterionic, ACE is zero charge (with a protonated phenol group), and NPX is negatively charged. Meanwhile, the adsorbent has a pH_{PZC} between 2.0 and 4.0, so it has negative and positive charges.

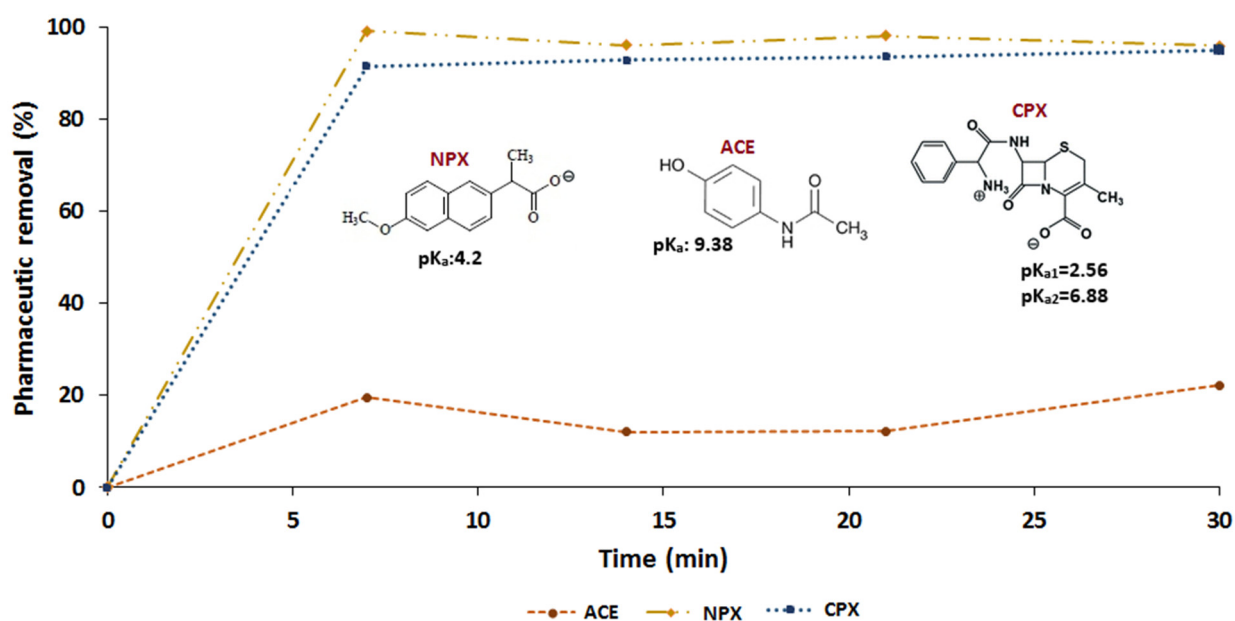


Figure 4. Adsorption of naproxen (NPX), acetaminophen (ACE), and cephalexin (CPX) on F_{Zn} material. Adsorption conditions (pharmaceutical): 20 mg L^{-1} ; adsorbent doses: 1.6 g L^{-1} ; pH: 4.0–5.0.

Thus, the high removal efficiencies for CPX and NPX can be attributed to electrostatic interactions with the adsorbent that are not present with ACE under the working conditions. The 20% removal efficiency of ACE can be related to other types of interactions such as hydrogen bonds, π - π interactions, or complexation [5], which should also contribute to the removal of CPX and NPX. According to Boehm titration (Table 1), the adsorbent has phenolic groups on its surface, which have the ability to form a complex with the carboxylic unprotonated group of NPX or CPX and through hydrogen bonds with the carbonyl group on ACE. Zeng et al., 2018 [5] found that hydrogen bonding is a dominant mechanism for the adsorption of the antibiotics doxycycline and ciprofloxacin on biochars. For F_{Zn} , electrostatic attraction appears to be the most important interaction compared with hydrogen bonds and π - π interactions.

2.4. Effect of Adsorbent Dose

Figure 5 shows the effect of the adsorbent dose on the CPX adsorption capacity (Q_e , which is Q_t at the equilibrium) and removal efficiency. The adsorbent dose was varied from 0.2 to 2 g L^{-1} under the favorable conditions previously determined. Increasing the adsorbent dose decreased the CPX adsorption capacity while increasing the CPX removal efficiency. As shown in Figure 5 the CPX adsorption capacity decreased from 50 mg g^{-1} to 10 mg g^{-1} , and the removal efficiency increased from 40% to 98%. The increase in the removal efficiency with the adsorbent dose can be attributed to the increased surface area and availability of more adsorption sites [26]. However, when the F_{Zn} dose is low, the fewer adsorption sites limit the increase in the removal efficiency, reducing the CPX removal efficiency [27]. At higher F_{Zn} doses, aggregation limits the number of active surface sites, which slows the increase in the removal efficiency and reduces the adsorption capacity [28].

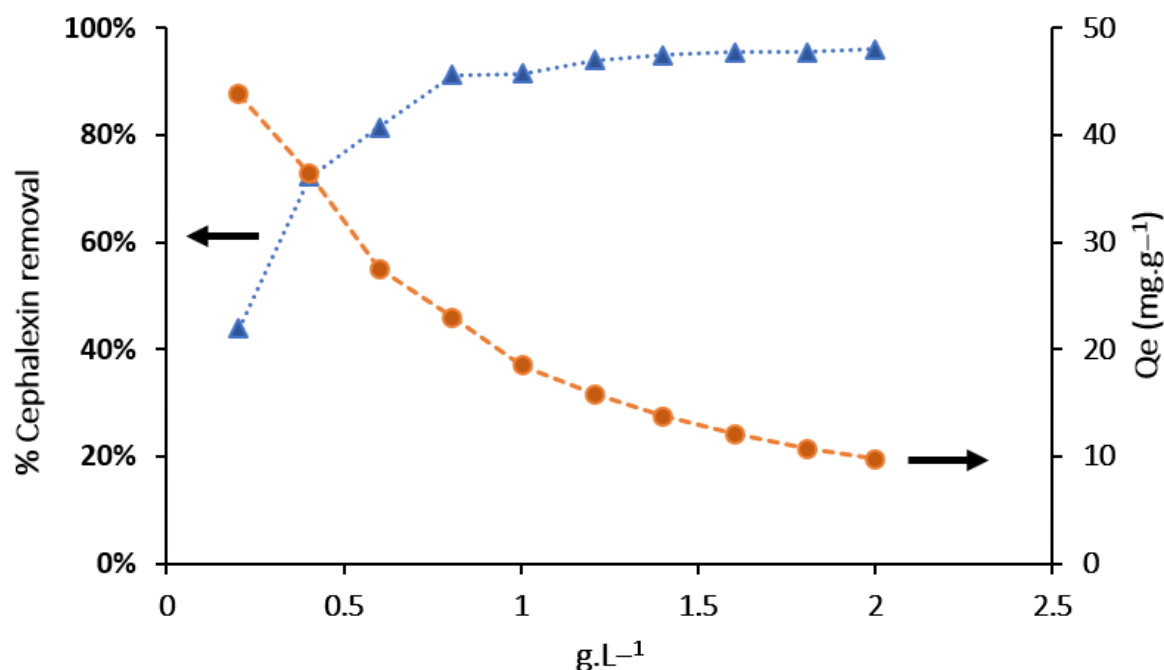


Figure 5. Effect of adsorbent dosage on the adsorption capacity and percentage removal of CPX (adsorption conditions: (CFX): 20 mg L⁻¹, time: 180 min).

The optimum adsorbent dose was determined to be 1.6 g L⁻¹ because this was the minimum dose with the highest removal efficiency and stable adsorption capacity. Similar results have been reported for CPX removal by other activated carbonaceous materials [2,9,29]. These studies also observed that the removal efficiency rapidly increased and the equilibrium adsorption capacity decreased as the adsorbent dose was increased up to 1.6 g/L, after which both the removal efficiency and adsorption capacity remained unchanged [2,5].

2.5. Adsorption Kinetics

Adsorption kinetics can be used to predict the removal efficiency for a contaminant from an aqueous solution. Controlling factors can be determined, such as the rate of chemical reactions and the mass transfer mechanism. In this study, the PFO [30], PSO [31], and intra-particle diffusion [32] models were used to evaluate the adsorption of different concentrations of CPX on F_{Zn}. The lineal equations of the PFO and PSO models can be expressed as follows:

$$\log(q_e - q_t) = \log q_e - \frac{k_1}{2.303}t \quad (1)$$

$$\frac{t}{q_t} = \frac{1}{k_2 q_e^2} + \frac{t}{q_e} \quad (2)$$

where q_t and q_e are the adsorption capacities of CPX at time t and at equilibrium, respectively (mg g⁻¹); t is the reaction time (min); and k_1 and k_2 are the adsorption rate constants of PFO and PSO, respectively (g mg⁻¹ min⁻¹). q_e and the rate constants of the PFO and PSO models can be determined from the slope and intercept of the plot of $\log(q_e - q_t)$ versus t and t/q_t versus t . Figure S2 (Supporting Information) shows the lineal equation adjusted for each model. The intra-particle diffusion rate parameter can be expressed as follows:

$$q_t = k_{di}\sqrt{t} + C_i \quad (3)$$

The intra-particle diffusion rate constant k_{di} (mg g⁻¹ min^{-1/2}) and C_i can be calculated from the slope and intercept of these plots. For all concentrations in this study, the correlation coefficient (R^2) and normalized standard deviation (Δq_e , %) given in Table 2

indicated that the PSO model fit the experimental data better than the PFO model did. This indicates that the adsorption process can be attributed to chemical adsorption [10] through electron sharing or transfer between F_{Zn} and CPX. These results are consistent with other studies on the adsorption of pharmaceuticals on carbonaceous materials [6,12,13,33,34]. Figure S3 (Supporting Information) shows the effect of the initial concentration of CPX on the removal efficiency.

Table 2. Adsorption kinetic parameters of CPX onto F_{Zn} (adsorbent doses: 1.6 g L^{-1} , pH: 5 to 6; contact time: 60 min).

	Initial Concentration						
	10 mg L^{-1}	15 mg L^{-1}	20 mg L^{-1}	25 mg L^{-1}	35 mg L^{-1}	50 mg L^{-1}	70 mg L^{-1}
Experimental q_e (mg g^{-1})	5.64	8.51	11.86	14.76	18.36	26.50	37.68
	Pseudo-First Order						
q_e (mg g^{-1})	—	0.59	1.12	1.68	4.68	6.18	3.39
k_1 (min^{-1})	—	0.03	0.04	0.04	0.07	0.07	0.04
Δq_e (%)	—	93	91	89	74	77	91
R^2	—	0.969	0.999	0.990	0.989	0.928	0.889
	Pseudo-Second Order						
q_e (mg g^{-1})	5.68	8.56	12.0	14.8	18.9	27.3	38.17
k_2 (min^{-1})	0.19	0.15	0.09	0.07	0.03	0.02	0.28
Δq_e (%)	0.59	0.54	1.56	0.24	2.8	2.8	1.28
R^2	0.999	1	1	0.999	1	0.999	0.999
	Intraparticle Diffusion Model						
k_{d1}	0.146	0.146	0.164	0.224	1.073	1.351	0.7947
C_1	4.756	7.537	10.68	12.94	12.56	18.52	32.45
R^2	0.981	0.979	0.999	0.942	0.988	0.931	0.9751
k_{d2}	0.022	0.033	−0.008	0.055	0.297	0.428	0.455
C_2	5.39	8.160	11.945	14.163	16.077	23.234	34.18
R^2	0.831	0.980	0.7913	0.999	0.9812	0.9583	0.993

The CPX removal efficiency increased remarkably with an increase in the initial concentration. During the initial step, the adsorption rate was high owing to the driving forces from the high concentration and huge number of active sites. The intra-particle diffusion model was used to describe the diffusion of CPX molecules onto F_{Zn} . According to Equation (3), if the linear trend line fit to q_t versus $t^{0.5}$ passes through the origin point (i.e., $C_i = 0$), the intra-particle diffusion is the only rate-limiting step for the adsorption kinetics. As demonstrated in Table 2, all calculated C_i values were greater than zero, indicating that more than one mechanism controlled the adsorption process. The adsorption rate constants for the first adsorption stage (K_{1d}) were higher than those for the second adsorption stage (K_{2d}). This indicates that the external diffusion of CPX molecules from the solution to the adsorbent surface was faster than the diffusion of CPX molecules onto the adsorbent pores. This also indicates that the rate of CPX adsorption was initially faster because of the availability of more active sites at the beginning of the adsorption process.

2.6. Isotherm Studies

Adsorption isotherm models describe the distribution of the adsorbed contaminant on the adsorbent after the equilibrium state is reached. The information provided by these models is very important to understand the adsorption process. In this study, the Langmuir [35] and Freundlich [36] models were applied to analyze the experimental data. The Langmuir isotherm assumes monolayer adsorption and is widely used to quantify the maximum adsorption capacity (Q_m):

$$\frac{C_e}{Q_e} = \frac{1}{Q_m K_L} + \frac{C_e}{Q_m} \quad (4)$$

where Q_m is the maximum adsorption capacity (mg g^{-1}) and C_e and Q_e are the equilibrium CPX concentration (mg L^{-1}) and equilibrium adsorption capacity (mg CPX g^{-1} of F_{Zn}), respectively. Q_m and the constant K_L (L g^{-1}) can be calculated from the slope and intercept (Figure S4, Supporting Information). The Langmuir isotherm can be used to determine the degree of affinity between CPX and F_{Zn} :

$$R_L = \frac{1}{1 + C_e K_L} \quad (5)$$

The Freundlich isotherm model assumes multilayer adsorption, and it is often used for heterogeneous surfaces. A linear form of the Freundlich equation is given by [37]

$$\log Q_e = \log K_F + \frac{1}{n} \log C_e \quad (6)$$

where Q_e is the equilibrium adsorption capacity (mg g^{-1}); n (g L^{-1}) and K_F are the adsorption intensity (i.e., degree of adsorption favorability) and adsorption capacity, respectively; and C_e is the concentration (mg L^{-1}).

Figure 6 shows the experimental and theoretical isotherms of CPX on F_{Zn} . The adsorption capacity increased with the equilibrium concentration at $0\text{--}12 \text{ mg L}^{-1}$. At $R^2 = 0.98$, the Langmuir model best described the experimental data of CPX adsorption on F_{Zn} , which suggests monolayer adsorption (see Figure S4 and Table S1, Supporting information).

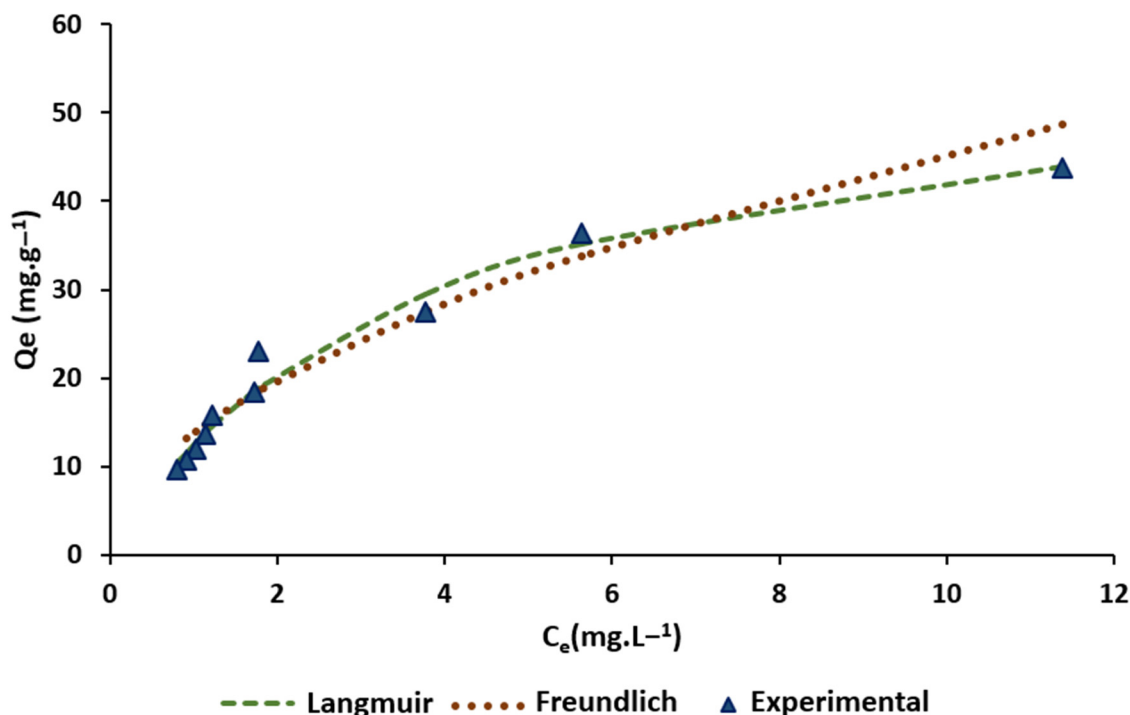


Figure 6. Experimental and theoretical isotherm values of CPX on F_{Zn} (180 min: adsorbent amount 0.02 to 0.2 g).

The Langmuir separation factor (R_L) in Equation (5) was used to determine if the adsorption process was irreversible ($R_L = 0$), linear ($R_L = 1$), favorable ($0 < R_L < 1$), or unfavorable ($R_L > 1$) [38]. In this study, $R_L = 0.15$ was considered to indicate that the CPX adsorption on F_{Zn} was favorable. The maximum monolayer adsorption capacity (Q_m) was 57.47 mg/g , which is comparable to values reported for CPX adsorption with several types of biomass (Table 3).

Table 3. Comparison of maximum adsorption capacity of CPX using biomass-derived adsorbents.

Biochar	Q_m (mg g ⁻¹)	Reference
Fiber Palm	57.47	This study
Alligator weed	45.00	[2]
pomegranate peel	87.18	[38]
Albizia lebbbeck seed pods	118.08	[9]

2.7. Thermodynamic Behavior

To evaluate the thermodynamic parameters for CPX adsorption on F_{Zn}, experiments were carried out at 15, 25, and 35 °C. Kinetic data obtained by the PSO model such as k_2 were used with the Arrhenius equation to obtain the activation energy E_a (kJ mol⁻¹) [39,40]:

$$\ln k_2 = \ln A_0 - \frac{E_a}{RT} \quad (7)$$

where A_0 is the Arrhenius constant, R is the universal gas constant (8.314 J mol⁻¹ K⁻¹), and T is the temperature (K). E_a is defined as the minimal energy that CPX overcomes for adsorption and was calculated from the slope of the plot $\ln k_2$ versus $1/T$ to be 91.6 kJ mol⁻¹ (see Figure S5A).

According to previous studies, a low activation energy of 5–50 kJ mol⁻¹ suggests physical adsorption, whereas $E_a > 50$ kJ mol⁻¹ implies chemical adsorption. Therefore, the obtained E_a value indicates that chemisorption is the predominant mechanism for CPX adsorption on F_{Zn}. This agrees with the fit to the PSO model and with the electrostatic interaction and influence of functional groups, as previously discussed.

The thermodynamic parameters of the standard free energy (ΔG°), enthalpy (ΔH°), and entropy (ΔS°) were determined as follows [39,41]:

$$\ln k_c = \frac{\Delta S}{R} - \frac{\Delta H}{RT} \quad (8)$$

$$\Delta G_{ads} = \Delta H_{ads} - T\Delta S_{ads} \quad (9)$$

where R (8.314 J/mol K) is the ideal gas constant, T (K) is the temperature, and k_c (L/g) is the standard thermodynamic equilibrium constant defined by qe/Ce . ΔH° and ΔS° can be estimated from the slope and intercept, respectively, for the plot of $\ln k_c$ versus $1/T$ (see Figure S5B).

Table 4 demonstrates that ΔG° became more negative as the temperature increased. This indicates that CPX adsorption is a spontaneous process favored by increasing temperature. The positive ΔS° confirmed the increased randomness at the solid–solution interface during the removal process [42]. The positive ΔH° indicates that the adsorption is endothermic in nature and that it is more favorable at higher temperatures. This may be related to the CPX interaction with active sites on the adsorbent surface, such as functional groups, or increased intra-particle diffusion within pores. Similar results have been reported for the removal of tetracycline with biochar [27] and hydrochar [43], where the adsorption was found to be a spontaneous and endothermic process.

Table 4. Thermodynamic parameters of CPX adsorption on palm fiber adsorbent.

Temperature (°C)	Activation Energy, E_a (kJ/mol)	ΔH° (kJ/mol)	ΔS° (J/mol)	ΔG° (kJ/mol)
15				−3.65
25	91.6	62.2	228.5	−5.93
30				−7.08

2.8. Adsorption Process

Figure 7 describes the probable interactions between the antibiotic and adsorbent. The results obtained by Boehm titration, IR analysis, and changes in CPX removal efficiency with pH suggest three main interactions between the adsorbent and CPX, namely, hydrogen bonds, electrostatic interactions, and π - π interaction.

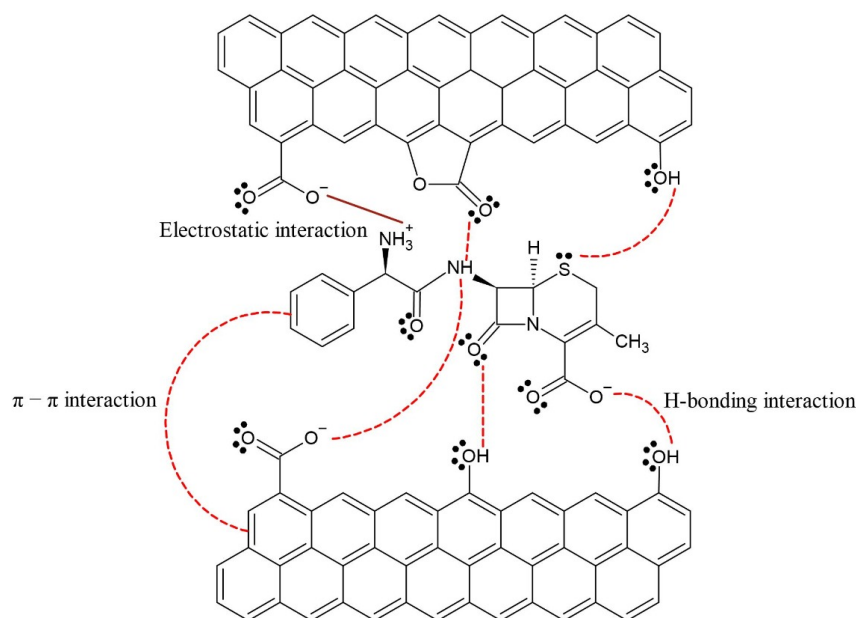


Figure 7. Possible interactions during CPX removal at pH: 4–5.

The Boehm titration results (see Table 1) indicate the presence of oxygenated groups such as phenols, carboxylic acids, and quinones. This is supported by the FT-IR results for the adsorbent (Figure S1A). The presence of phenolic groups in the adsorbent suggests possible hydrogen bonding with the amino, thiol, and carboxylate groups of CPX. Electrostatic interactions are generated between the carboxylates of the adsorbent and protonated amines on CPX. These interactions were evident in the FT-IR analysis (Figure S1A), where a decrease in the band of the $-OH$ group (phenols and carboxylic acids) was observed in the adsorbent after CPX adsorption. The above results agree with the removal efficiencies observed with the change in pH. At $pH < 6$ (removal efficiency of $\sim 90\%$), electrostatic interactions between deprotonated carboxylic acid and the protonated amino groups of CPX were predominant. At $pH > 8$, both the CPX and adsorbent were negatively charged, which generated electrostatic repulsion and agrees with the CPX removal efficiency of around 20%. In this case, the low removal efficiency was due to hydrogen bonding of the phenol in the adsorbent with the sulfur, nitrogen, and oxygen of CPX.

Other authors have shown that the oxygenated groups of the adsorbent participate in adsorption processes [6]. For example, [2] suggested that the oxygen-containing functional groups of the adsorbent, including hydroxyl, carboxyl, and alkoxy groups, may participate in the adsorption of antibiotics by forming hydrogen bonds with the phenolic hydroxyl, carboxyl, and amino groups of doxycycline and ciprofloxacin. Other interactions that contribute to CPX adsorption include the π - π interactions generated between the aromatic ring of CPX and aromatic fraction of the adsorbent, as evidenced by the displacement of the peaks of the aromatic $C=C$ bonds around 1600 cm^{-1} after CPX adsorption. Similar results were reported by [5], who demonstrated the role of π - π interactions by preparing adsorbents with varying aromatic contents and showing that those with a higher aromatic fraction had a higher adsorption capacity. The above interactions were used to analyze the effects between components present in real matrices on CPX adsorption.

2.9. Effect of Complex Matrices on CFX Adsorption

Real wastewater has several components that may interfere with the adsorption process of the target molecule. In this study, the adsorption of CPX on F_{Zn} from traditional matrices such as wastewater and urine was evaluated. For comparison, CPX removal from distilled water was also considered. Table S2 (Supporting Information) presents the characteristics of each matrix. As shown in Figure 8, after 60 min, 71% and 77% of CPX were removed from the simulated wastewater and urine, respectively, while 96% of CPX was removed from the distilled water.

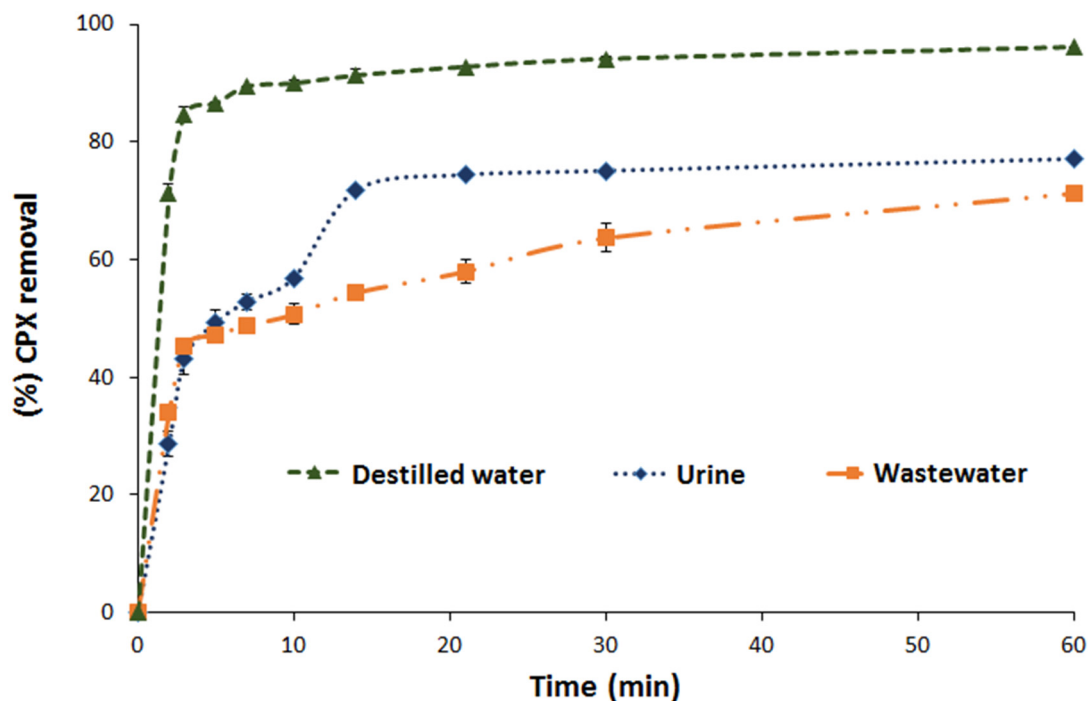


Figure 8. Adsorption of CPX in aqueous solution, in synthetic matrices of waste water and urine, using F_{Zn} (conditions: matrices doped with 25 mg L^{-1} of CPX, adsorbent dose 1.6 g L^{-1}).

As expected, the removal efficiency decreased for both complex matrices. The tested matrices were characterized by a high inorganic salt content. Under working pH conditions and considering the PZC, the adsorbent was negatively charged and favored cation adsorption. Hence, cations such as Na^+ , K^+ , Ca^{2+} , Mg^{2+} , and CPX may have competed for the active sites of the adsorbent (i.e., deprotonated carboxylic acids) [12]. On the other hand, the differences between the wastewater and urine were because the former had more cations. Despite the reduced CPX adsorption in these complex matrices, a removal efficiency of around 70% is quite good for actual applications.

3. Materials and Methods

3.1. Reagents

All reagents used in this study were of analytical grade. CPX ($\text{C}_{16}\text{H}_{17}\text{N}_3\text{O}_4\text{S}$) was purchased from Syntofarma and was used to prepare the synthetic solutions. HCl, NaOH, ZnCl_2 , and H_3PO_4 were purchased from Sigma-Aldrich (St. Louis, MO, USA).

3.2. Biochar Preparation

Fiber (F) and shell (S) residues from palm oil production were collected from CENI-PALMA (Villavicencio, Colombia), washed with distilled water to remove impurities, and dried in an oven at $110 \text{ }^\circ\text{C}$ for 3 h. F and S were activated with ZnCl_2 as per the previously reported procedure [19,44]. The activated adsorbents were designated as F_{Zn} and S_{Zn} , respectively. To evaluate the effect of the activating agent, F was alternatively impregnated

with H_3PO_4 , and this adsorbent was designated as F_{HA} . After preparation, all adsorbents were rinsed several times to reach a pH of 7. They were then dried in an oven at $110\text{ }^\circ\text{C}$, sieved to obtain a particle size of $<0.15\text{ mm}$, and stored in a dry place before use.

3.3. Biochar Characterization

The morphological properties of the adsorbents were characterized by scanning electron microscopy (SEM; Oxford Instruments, Concord, MA, USA). The surface area and pore volume were determined by nitrogen adsorption at 77 K with an ASAP 2020 Micrometrics instrument (Norcross, GA, USA.) according to the Brunauer–Emmett–Teller (BET) method [45]. Surface functional groups were analyzed by Fourier transform infrared (FT-IR) spectroscopy according to the attenuated total reflectance (ATR) (PerkinElmer, Waltham, MA, USA). Boehm titrations were performed following a standardized method to quantify the acidic groups on the adsorbent surface [19]. Finally, the point of zero charge (PZC) was obtained with the solid addition method.

3.4. Batch Adsorption Experiments

HCl (0.1 M) and NaOH (0.1 M) solutions were used to adjust the pH as required during the experiments. Adsorption experiments were carried out in batch mode. First, 100 mL of various initial concentrations of CPX and a certain amount of an adsorbent were placed into an Erlenmeyer flask and stirred constantly at 200 rpm. The effects of parameters such as the pH (2–12) at room temperature (298 K), adsorption time (0–60 min), CPX concentration ($10\text{--}70\text{ mg L}^{-1}$), and adsorbent dose ($0.5\text{--}2\text{ g L}^{-1}$) on the adsorption capacity were investigated. The adsorbent with the best performance was determined according to the CPX removal efficiency (%), as given in Equation (10), and the amount of CPX adsorbed at time t was calculated with Equation (11):

$$\text{CPX Removal (\%)} = \frac{C_0 - C_t}{C_0} \times 100\% \quad (10)$$

$$q_t = \frac{C_0 - C_t}{w} \times v \quad (11)$$

where q_t is the adsorption capacity of the adsorbent (mg/g); C_0 and C_t (mg/L) are the CPX concentrations in the solution initially and at time t , respectively; v is the solution volume (L); and w is the mass of the adsorbent (g). To examine the diffusion mechanism involved during the adsorption process, three kinetic models were considered, namely, the pseudo-first-order (PFO), pseudo-second-order (PSO), and intra-particle diffusion models. The data were also adjusted to the Langmuir and Freundlich isotherms. These models were applied to the best adsorbent according to Equation (10). The linear coefficient correlation (R^2 values) and the normalized standard deviation (Δq , %) were evaluated to select the appropriate kinetic and isotherm models that best describe the measured data, as given below:

$$\Delta q (\%) = 100 \sqrt{\frac{\sum \left(\frac{q_{\text{exp}} - q_{\text{cal}}}{q_{\text{exp}}} \right)^2}{N - 1}} \quad (12)$$

To evaluate the effect of the temperature on CPX adsorption, the thermodynamic parameters were studied at 15, 25, and $35\text{ }^\circ\text{C}$, where 0.16 g of adsorbent was added to 100 mL of CPX solution with a concentration of 20 mg L^{-1} . The effect of complex matrices was evaluated by adding 0.16 g of adsorbent to 100 mL of simulated municipal wastewater and urine (see composition in Table S2) doped with 20 mg L^{-1} CPX.

After the batch adsorption experiments, the samples were centrifuged and filtered with Whatman paper ($0.2\text{ }\mu\text{m}$). The residual CPX concentration was determined by high-performance liquid chromatography–ultraviolet (HPLC-UV) equipped with a reverse phase column (C18 column; annulus of 4.6 mm and length of 150 mm) and methanol carrier phase (30–70%) at a detection wavelength of 263 nm.

4. Conclusions

This study was focused on the understanding of the adsorption process of cephalexin onto biochar produced from fiber residue from palm oil activated with $ZnCl_2$. The main results are as follows:

F_{Zn} is an effective CPX adsorbent, even in complex matrices as wastewater and urine.

The data for CPX adsorption on the adsorbent F_{Zn} were better fitted to the Langmuir model, suggesting homogeneous and monolayer adsorption of the pharmaceutical on the adsorbent surface.

This process followed a PSO kinetic model, where the adsorption capacity was assumed as proportional to the square of the number of unoccupied sites. The adsorption process appears to be dominated by chemical adsorption through electron sharing or transfer between F_{Zn} and CPX.

The positive ΔH° indicates that the adsorption is endothermic and that it is more favorable at higher temperatures. This may be related to the CPX interacting with active sites on the adsorbent surface such as functional groups or the increased intra-particle diffusion within pores.

Based on the effects of the pH and pharmaceutical structure on the removal efficiency, the most likely adsorption mechanisms appear to be electrostatic interactions and hydrogen bonding, although π - π interactions also appear to contribute.

Finally, F_{Zn} was demonstrated to be a good adsorbent for charged pharmaceuticals, but was less effective for neutral substances.

This work also contributes to identifying the fiber residue from palm as a potential adsorbent to be applied for purifying wastewater that contains trace antibiotics.

Supplementary Materials: The following are available online, Figure S1: FTIR spectrum for adsorbent materials before and after CPX removal (A) F_{Zn} ; (B) F_{HA} ; (C) S_{Zn} . Figure S2: Lineal equation adjusted for the pseudo-first (PFO) and pseudo-second (PSO) kinetics models at different CPX concentrations. Figure S3: Effect of the initial concentration of CPX on the removal percent removal on F_{Zn} . [Experimental conditions: adsorbent doses: 1.6 g L^{-1} ; pH: natural]. Figure S4 (A) Freundlich and (B) Langmuir isotherm models for the adsorption of CPX onto F_{Zn} [20 mg L^{-1} , 180 min]. Figure S5: Thermodynamic parameters of CPX adsorption on palm fiber adsorbent (A) E_a and (B) Gibbs, Enthalpy and Entropy. Table S1: Parameters of isotherm models for the adsorption of CPX onto F_{Zn} [20 mg L^{-1} , 180 min], Table S2: Composition of simulated wastewater (pH: 6.5) and simulated aged urine (pH: 8.5).

Author Contributions: Conceptualization, N.A., J.P. and R.A.T.-P.; Data curation, S.M.L.; Formal analysis, N.A., S.M.L., J.P. and R.A.T.-P.; Funding acquisition, N.A., J.P. and R.A.T.-P.; Investigation, N.A., J.P. and R.A.T.-P.; Methodology, N.A., S.M.L., J.P. and R.A.T.-P.; Project administration, R.A.T.-P.; Resources, J.P. Supervision, N.A.; Validation, N.A.; Visualization, N.A., J.P. and R.A.T.-P.; Writing—original draft, N.A. and J.P.; Writing—review & editing, N.A., J.P. and R.A.T.-P. All authors have read and agreed to the published version of the manuscript.

Funding: The authors acknowledge Universidad de Medellín, Universidad de Antioquia, and Uniremington for financing the project, and the support provided by MINCIENCIAS COLOMBIA (before named COLCIENCIAS) through the project No. 111577757323.

Data Availability Statement: Data are available from the authors on request.

Acknowledgments: The authors would like to acknowledge Universidad de Medellín, Universidad de Antioquia, and Uniremington for supporting this research.

Conflicts of Interest: The authors declare no conflict of interest.

Sample Availability: Adsorbent samples are available from the authors.

References

1. Reza, R.A.; Ahmaruzzaman, M.; Sil, A.K.; Gupta, V.K. Comparative adsorption behavior of ibuprofen and clofibric acid onto microwave assisted activated bamboo waste. *Ind. Eng. Chem. Res.* **2014**, *53*, 9331–9339. [[CrossRef](#)]
2. Miao, M.S.; Liu, Q.; Shu, L.; Wang, Z.; Liu, Y.Z.; Kong, Q. Removal of cephalixin from effluent by activated carbon prepared from alligator weed: Kinetics, isotherms, and thermodynamic analyses. *Process Saf. Environ. Prot.* **2016**, *104*, 481–489. [[CrossRef](#)]
3. Watkinson, A.J.; Murby, E.J.; Kolpin, D.W.; Costanzo, S.D. The occurrence of antibiotics in an urban watershed: From wastewater to drinking water. *Sci. Total Environ.* **2009**, *407*, 2711–2723. [[CrossRef](#)] [[PubMed](#)]
4. Perea, L.A.; Palma-Goyes, R.E.; Vazquez-Arenas, J.; Romero-Ibarra, I.; Ostos, C.; Torres-Palma, R.A. Efficient cephalixin degradation using active chlorine produced on ruthenium and iridium oxide anodes: Role of bath composition, analysis of degradation pathways and degradation extent. *Sci. Total Environ.* **2019**, *648*, 377–387. [[CrossRef](#)]
5. Zeng, Z.W.; Tan, X.F.; Liu, Y.G.; Tian, S.R.; Zeng, G.M.; Jiang, L.H.; Liu, S.B.; Li, J.; Liu, N.; Yin, Z.H. Comprehensive adsorption studies of doxycycline and ciprofloxacin antibiotics by biochars prepared at different temperatures. *Front. Chem.* **2018**, *6*, 1–11. [[CrossRef](#)] [[PubMed](#)]
6. Mondal, S.; Patel, S. Naproxen Removal Capacity Enhancement by Transforming the Activated Carbon into a Blended Composite Material. *Water Air Soil Pollut.* **2020**, *231*, 37. [[CrossRef](#)]
7. Nazari, G.; Abolghasemi, H.; Esmaili, M.; Sadeghi Pouya, E. Aqueous phase adsorption of cephalixin by walnut shell-based activated carbon: A fixed-bed column study. *Appl. Surf. Sci.* **2016**, *375*, 144–153. [[CrossRef](#)]
8. Gundogdu, A.; Duran, C.; Senturk, H.B.; Soylak, M.; Ozdes, D.; Serencam, H.; Imamoglu, M. Adsorption of phenol from aqueous solution on a low-cost activated carbon produced from tea industry waste: Equilibrium, kinetic, and thermodynamic study. *J. Chem. Eng. Data* **2012**, *57*, 2733–2743. [[CrossRef](#)]
9. Ahmed, M.J.; Theydan, S.K. Adsorption of cephalixin onto activated carbons from Albizia lebeck seed pods by microwave-induced KOH and K₂CO₃ activations. *Chem. Eng. J.* **2012**, *211–212*, 200–207. [[CrossRef](#)]
10. Mohammed, A.A.; Kareem, S.L. Adsorption of tetracycline from wastewater by using Pistachio shell coated with ZnO nanoparticles: Equilibrium, kinetic and isotherm studies. *Alex. Eng. J.* **2019**, *58*, 917–928. [[CrossRef](#)]
11. Jang, H.M.; Kan, E. Engineered biochar from agricultural waste for removal of tetracycline in water. *Bioresour. Technol.* **2019**, *284*, 437–447. [[CrossRef](#)] [[PubMed](#)]
12. Paredes-Laverde, M.; Silva-Agredo, J.; Torres-Palma, R.A. Removal of norfloxacin in deionized, municipal water and urine using rice (*Oryza sativa*) and coffee (*Coffea arabica*) husk wastes as natural adsorbents. *J. Environ. Manag.* **2018**, *213*, 98–108. [[CrossRef](#)]
13. Paredes-Laverde, M.; Salamanca, M.; Silva-Agredo, J.; Manrique-Losada, L.; Torres-Palma, R.A. Selective removal of acetaminophen in urine with activated carbons from rice (*Oryza sativa*) and coffee (*Coffea arabica*) husk: Effect of activating agent, activation temperature and analysis of physical-chemical interactions. *J. Environ. Chem. Eng.* **2019**, *7*, 103318. [[CrossRef](#)]
14. Garcia-Nunez, J.A.; Ramirez-Contreras, N.E.; Rodriguez, D.T.; Silva-Lora, E.; Frear, C.S.; Stockle, C.; Garcia-Perez, M. Evolution of palm oil mills into bio-refineries: Literature review on current and potential uses of residual biomass and effluents. *Resour. Conserv. Recycl.* **2016**, *110*, 99–114. [[CrossRef](#)]
15. Giraldo, S.; Robles, I.; Ramirez, A.; Flórez, E.; Acelas, N. Mercury removal from wastewater using agroindustrial waste adsorbents. *SN Appl. Sci.* **2020**, *2*. [[CrossRef](#)]
16. Guechi, E.K.; Hamdaoui, O. Evaluation of potato peel as a novel adsorbent for the removal of Cu(II) from aqueous solutions: Equilibrium, kinetic, and thermodynamic studies. *Desalin. Water Treat.* **2016**, *57*, 10677–10688. [[CrossRef](#)]
17. Omoriyekomwan, J.E.; Tahmasebi, A.; Zhang, J.; Yu, J. Formation of hollow carbon nanofibers on bio-char during microwave pyrolysis of palm kernel shell. *Energy Convers. Manag.* **2017**, *148*, 583–592. [[CrossRef](#)]
18. Foo, K.Y.; Hameed, B.H. Microwave assisted preparation of activated carbon from pomelo skin for the removal of anionic and cationic dyes. *Chem. Eng. J.* **2011**, *173*, 385–390. [[CrossRef](#)]
19. Giraldo, S.; Ramirez, A.P.; Flórez, E.; Acelas, N.Y. Adsorbent materials obtained from palm waste and its potential use for contaminants removal from aqueous solutions. *J. Phys. Conf. Ser.* **2019**, *1386*. [[CrossRef](#)]
20. Delgado-Moreno, L.; Bazhari, S.; Gasco, G.; Méndez, A.; El Azzouzi, M.; Romero, E. New insights into the efficient removal of emerging contaminants by biochars and hydrochars derived from olive oil wastes. *Sci. Total Environ.* **2021**, *752*. [[CrossRef](#)]
21. Mohammed, A.A.; Al-Musawi, T.J.; Kareem, S.L.; Zarrabi, M.; Al-Ma'abreh, A.M. Simultaneous adsorption of tetracycline, amoxicillin, and ciprofloxacin by pistachio shell powder coated with zinc oxide nanoparticles. *Arab. J. Chem.* **2019**, *13*, 4629–4643. [[CrossRef](#)]
22. Krasucka, P.; Pan, B.; Sik Ok, Y.; Mohan, D.; Sarkar, B.; Oleszczuk, P. Engineered biochar—A sustainable solution for the removal of antibiotics from water. *Chem. Eng. J.* **2021**, *405*, 126926. [[CrossRef](#)]
23. Grisales-Cifuentes, C.M.; Serna Galvis, E.A.; Porras, J.; Flórez, E.; Torres-Palma, R.A.; Acelas, N. Kinetics, isotherms, effect of structure, and computational analysis during the removal of three representative pharmaceuticals from water by adsorption using a biochar obtained from oil palm fiber. *Bioresour. Technol.* **2021**, *326*, 124753. [[CrossRef](#)] [[PubMed](#)]
24. Ooi, C.H.; Cheah, W.K.; Sim, Y.L.; Pung, S.Y.; Yeoh, F.Y. Conversion and characterization of activated carbon fiber derived from palm empty fruit bunch waste and its kinetic study on urea adsorption. *J. Environ. Manag.* **2017**, *197*, 199–205. [[CrossRef](#)]
25. Khanday, W.A.; Ahmed, M.J.; Okoye, P.U.; Hummadi, E.H.; Hameed, B.H. Single-step pyrolysis of phosphoric acid-activated chitin for efficient adsorption of cephalixin antibiotic. *Bioresour. Technol.* **2019**, *280*, 255–259. [[CrossRef](#)] [[PubMed](#)]

26. Nazari, G.; Abolghasemi, H.; Esmaili, M. Batch adsorption of cephalexin antibiotic from aqueous solution by walnut shell-based activated carbon. *J. Taiwan Inst. Chem. Eng.* **2016**, *58*, 357–365. [[CrossRef](#)]
27. Zhang, P.; Li, Y.; Cao, Y.; Han, L. Characteristics of tetracycline adsorption by cow manure biochar prepared at different pyrolysis temperatures. *Bioresour. Technol.* **2019**, *285*, 121348. [[CrossRef](#)]
28. Anwar, J.; Shafique, U.; Salman, M.; Dar, A.; Anwar, S. Removal of Pb(II) and Cd(II) from water by adsorption on peels of banana. *Bioresour. Technol.* **2010**, *101*, 1752–1755. [[CrossRef](#)]
29. Naghipour, D.; Amouei, A.; Estaji, M.; Taghavi, K.; Allahabadi, A. Cephalexin adsorption from aqueous solutions by biochar prepared from plantain wood: Equilibrium and kinetics studies. *Desalin. Water Treat.* **2019**, *143*, 374–381. [[CrossRef](#)]
30. Lagergren, S. Zur theorie der sogenannten adsorption gelöster Stoffe. Stockholm Kongl. svenska vetenskaps-akad. *Handlingar* **1898**. [[CrossRef](#)]
31. Ho, Y.S.; McKay, G. Kinetic models for the sorption of dye from aqueous solution by wood. *Process Saf. Environ. Prot.* **1998**, *76*, 183–191. [[CrossRef](#)]
32. Weber, W.J.; Morris, J.C. Kinetics of Adsorption on Carbon from Solution. *J. Sanit. Eng. Div.* **1963**, *89*, 31–60. [[CrossRef](#)]
33. Afshin, S.; Rashtbari, Y.; Ramavandi, B.; Fazlzadeh, M.; Vosoughi, M.; Mokhtari, S.A.; Shirmardi, M.; Rehman, R. Magnetic nanocomposite of filamentous algae activated carbon for efficient elimination of cephalexin from aqueous media. *Korean J. Chem. Eng.* **2020**, *37*, 80–92. [[CrossRef](#)]
34. Samarghandi, M.R.; Al-Musawi, T.J.; Mohseni-Bandpi, A.; Zarrabi, M. Adsorption of cephalexin from aqueous solution using natural zeolite and zeolite coated with manganese oxide nanoparticles. *J. Mol. Liq.* **2015**, *211*, 431–441. [[CrossRef](#)]
35. Armbruster, M.H.; Austin, J.B. The Adsorption of Gases on Plane Surfaces of Mica. *J. Am. Chem. Soc.* **1938**, *60*, 467–475. [[CrossRef](#)]
36. Freundlich, H. Over the adsorption in solution. *J. Phys. Chem.* **1906**, *57*, 385–471.
37. Ramirez, A.; Ocampo, R.; Giraldo, S.; Padilla, E.; Flórez, E.; Acelas, N. Removal of Cr (VI) from an aqueous solution using an activated carbon obtained from teakwood sawdust: Kinetics, equilibrium, and density functional theory calculations. *J. Environ. Chem. Eng.* **2020**, *8*, 103702. [[CrossRef](#)]
38. Rashtbari, Y.; Hazrati, S.; Azari, A.; Afshin, S.; Fazlzadeh, M.; Vosoughi, M. A novel, eco-friendly and green synthesis of PPAC-ZnO and PPAC-nZVI nanocomposite using pomegranate peel: Cephalexin adsorption experiments, mechanisms, isotherms and kinetics. *Adv. Powder Technol.* **2020**. [[CrossRef](#)]
39. Roy, A.; Adhikari, B.; Majumder, S.B. Equilibrium, kinetic, and thermodynamic studies of azo dye adsorption from aqueous solution by chemically modified lignocellulosic jute fiber. *Ind. Eng. Chem. Res.* **2013**, *52*, 6502–6512. [[CrossRef](#)]
40. Sajab, M.S.; Chia, C.H.; Zakaria, S.; Jani, S.M.; Ayob, M.K.; Chee, K.L.; Khiew, P.S.; Chiu, W.S. Citric acid modified kenaf core fibres for removal of methylene blue from aqueous solution. *Bioresour. Technol.* **2011**, *102*, 7237–7243. [[CrossRef](#)] [[PubMed](#)]
41. Bentouami, A.; Ouali, M.S. Cadmium removal from aqueous solutions by hydroxy-8 quinoleine intercalated bentonite. *J. Colloid Interface Sci.* **2006**, *293*, 270–277. [[CrossRef](#)] [[PubMed](#)]
42. Chia, C.H.; Duong, T.D.; Nguyen, K.L.; Zakaria, S. Thermodynamic aspects of sorption of Fe²⁺ onto unbleached kraft fibres. *J. Colloid Interface Sci.* **2007**, *307*, 29–33. [[CrossRef](#)] [[PubMed](#)]
43. Zhu, X.; Liu, Y.; Qian, F.; Zhou, C.; Zhang, S.; Chen, J. Preparation of magnetic porous carbon from waste hydrochar by simultaneous activation and magnetization for tetracycline removal. *Bioresour. Technol.* **2014**, *154*, 209–214. [[CrossRef](#)] [[PubMed](#)]
44. Ramírez, A.P.; Giraldo, S.; Flórez, E.; Acelas, N. Preparación de carbón activado a partir de residuos de palma de aceite y su aplicación para la remoción de colorantes Preparation of activated carbon from palm oil wastes and their application for methylene blue removal Abstract Preparação de carvão ativa. *Afinidad* **2012**, *559*, 203–210. [[CrossRef](#)]
45. Brunauer, S.; Emmett, P.H.; Teller, E. Adsorption of Gases in Multimolecular Layers. *J. Am. Chem. Soc.* **1938**, *60*, 309–319. [[CrossRef](#)]